Available online at www.sciencedirect.com

ScienceDirect

PHOTONICS AND NANOSTRUCTURES Fundamentals and Applications

Photonics and Nanostructures – Fundamentals and Applications 12 (2014) 376–386

www.elsevier.com/locate/photonics

THz metamaterials made of phonon-polariton materials

M. Kafesaki [a,b,*], A.A. Basharin [a], E.N. Economou [a,c], C.M. Soukoulis [a,d]

[a] *Institute of Electronic Structure and Laser, Foundation for Research and Technology, Hellas (FORTH), P.O. Box 1385, Heraklion, Crete, Greece*
[b] *Department of Materials Science and Technology, University of Crete, Greece*
[c] *Physics Department, University of Crete, Greece*
[d] *Ames Lab and Department of Physics and Astronomy, Iowa State University, Ames, IA, USA*

Received 24 March 2014; received in revised form 14 May 2014; accepted 28 May 2014
Available online 10 June 2014

Abstract

In this paper, we demonstrate numerically various phenomena and possibilities that can be realized in THz metamaterials made of phonon-polariton materials. Such phenomena include hyperbolic dispersion relation, subwavelength imaging using backward propagation and backward radiation, total transmission and subwavelength guiding exploiting Mie-resonant scattering in permittivity near zero host, and toroidal dipolar response. The systems that we use to demonstrate most of these phenomena are two-dimensional periodic systems of μm-scale rods in a host, where both rods and host are made of polaritonic alkali-halide materials.

1. Introduction

The continuously expanding technologies for THz sources along with the unique properties and capabilities of the THz radiation, especially in the security, sensing and communications domains, constantly increase nowadays the demand for the realization of components for the manipulation of THz waves [1,2].

Since the majority of natural materials do not show strong response to the THz waves, and so they do not offer themselves for THz handling and a straightforward THz component realization, metamaterials (i.e. artificial materials, structured in subwavelength scales and showing novel and unique properties, unattainable in natural materials), can offer an excellent solution to the problem. This is because the metamaterials response is based mainly on geometry-induced resonances [3] which can be easily tuned in frequency by adjusting the size of their basic building blocks. Moreover, the richness in the phenomena and properties achievable with metamaterials (like, e.g. very large, near zero or negative permittivity and/or permeability [3], negative refractive index [4,5], giant chirality [6,7] etc.) leads to a variety of capabilities for the metamaterial-based systems [8], including perfect absorption [9,10], subwavelength resolution imaging [11], polarization filtering and manipulation [12], spatial and temporal filtering, etc., which can be greatly exploited in the THz domain.

The majority of today's THz metamaterials use metal as the basic material for the metamaterials elements. There, the desired metamaterial property is achieved by properly designed current resonances in the subwavelength-size metallic elements (known as meta-atoms). An alternative option to achieve useful and interesting metamaterial properties is to use meta-atoms

* Corresponding author at: Foundation for Research and Technology, Hellas (FORTH), P.O. Box 1385, Heraklion, Crete, Greece.
Tel.: +30 2810 391547; fax: +30 2810 391569.
E-mail address: kafesaki@iesl.forth.gr (M. Kafesaki).

http://dx.doi.org/10.1016/j.photonics.2014.05.009
1569-4410/

made of a high-index dielectric, instead of a metal, and exploit the Mie-resonances of the meta-atom [13,14]. Due to the high-index of the meta-atom these resonances appear at wavelengths much larger than the meta-atom size, allowing thus the treatment of the total metamaterial as a homogeneous material with effective properties. A category of materials which in the THz regime combines both the properties and capabilities of metals and of high index dielectrics, and therefore provides an excellent candidate for THz metamaterial building blocks, is polaritonic materials [15]. Polaritonic materials are polar crystals where the incident radiation excites crystal vibrations (transverse optical phonons) in the crystal. The coupling of the incident radiation with the induced field created by the crystal vibrations results to the so-called phonon-polariton modes, and is described by a resonant permittivity response of Lorenz type:

$$\bar{\varepsilon} = \varepsilon_\infty \left(1 - \frac{\omega_L^2 - \omega_T^2}{\omega^2 - \omega_T^2 + i\omega\gamma}\right) \quad (1)$$

In Eq. (1) ω_T is the angular frequency of the transverse optical phonons in the crystal, which falls in the THz regime and at which the permittivity blows up (in the absence of losses), ω_L is the angular frequency of the longitudinal optical phonons in the crystal ($\omega_L > \omega_T$), and ε_∞ is the limiting value of the permittivity for high frequencies, well above ω_L but well below the electronic gap. The values of ω_T, ω_L and ε_∞ are related to the parameters of the polar crystal.

The dielectric function (1), in the frequency regime just above the resonance frequency, ω_T, shows negative values, similar to that of the dielectric function of metals in the optical regime (see, e.g. Fig. 1). This indicates that all the effects that can be observed in metal optics (plasmonics, optical metamaterials) can be transferred to the THz using polaritonic materials [16–19], something that offers to the polaritonic materials unique power for THz wave manipulation. Moreover, the high positive values of the dielectric function just below the resonance frequency, reaching in some cases values even of the order of few hundreds (e.g. for $LiTaO_3$ and TlCl) [20], can be exploited in a variety of high-index-based metamaterial phenomena, such as negative effective permeability and/or permittivity, negative refractive index, etc. [14,20–24]. Another particularly interesting frequency region encountered in polaritonic materials is where the dielectric function gets values close to zero, i.e. for frequencies around the frequency of longitudinal optical phonons, ω_L. The electromagnetic (EM) response of materials with epsilon near zero (ENZ) has been studied extensively recently, mainly in connection to metamaterials (since metamaterials can easily allow such kind of response), and interesting phenomena and possibilities have been proposed and demonstrated. Such phenomena include possibility to squeeze EM waves at will using narrow ENZ channels [25,26], possibility to easily shape the radiation pattern of sources embedded or in close proximity to ENZ structures [27], strong interaction of phonons with charge carriers resulting to instabilities generating THz waves [28,29], and others [30].

This broad range of permittivity values achievable in polaritonic materials is of great importance if such materials are properly shaped, providing metamaterial elements. Combining the rich shaping possibilities achievable by the modern fabrication approaches with the wide range of permittivity values achievable in polaritonic materials, one can result in a uniquely rich variety of phenomena which can have a great impact in all the modern THz applications. In this work we demonstrate numerically few of such phenomena, i.e. phenomena observable in metamaterials made of phonon-polariton materials, called here polaritonic metamaterials. In particular, we demonstrate: (a) hyperbolic dispersion relation response in anisotropic polaritonic metamaterials (see Section 3), leading to subwavelength resolution imaging; (b) subwavelength imaging and guiding due to backward radiation in polaritonic waveguides (see Section 4); (c) total transmission and extremely subwavelength guiding in metamaterials made of dielectric cylinders in an ENZ polaritonic host (see Section 5); (d) toroidal response in periodic systems built by proper clusters of polaritonic cylinders (as building blocks), due to the high epsilon response of the cylinders (see Section 6). The basic systems and materials that we use to demonstrate the above mentioned phenomena, as well as the simulation approaches employed, are discussed in the next section.

2. Basic systems and their electromagnetic properties

The systems that we will employ to demonstrate most of the polaritonic metamaterial based phenomena discussed here are alkali-halide polaritonic systems composed of LiF rods embedded in either NaCl or KCl host, in hexagonal periodic arrangement [31]. A drawing of such a system is shown in Fig. 1(a), while Fig. 1(b) shows the relative dielectric function of LiF and NaCl [16]. The dielectric function of KCl is very similar to that of NaCl, with the polaritonic resonance appearing at around 4.2 THz [16]. An important merit of those systems is that they can be easily fabricated in micro-meter

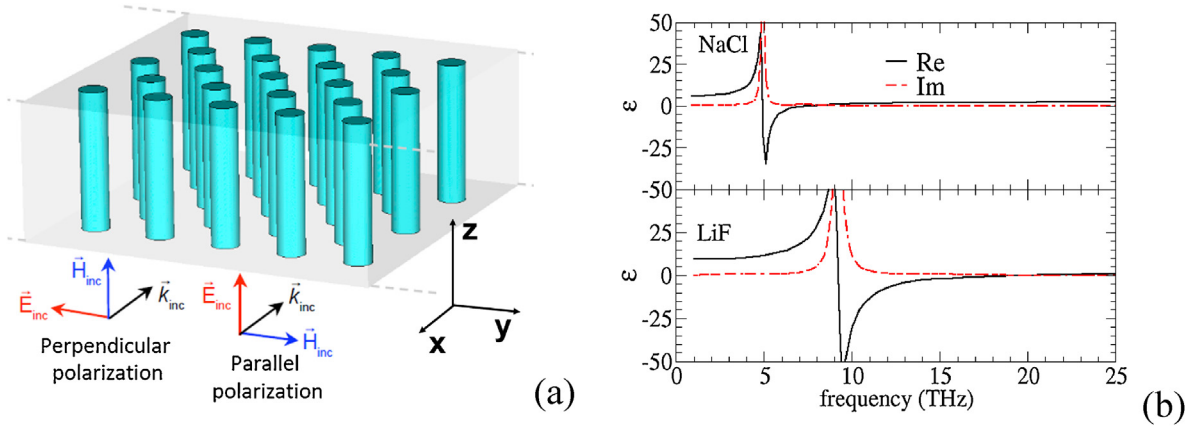

Fig. 1. (a) The geometry of the polaritonic rods embedded in a polaritonic host system and the polarizations of the incoming EM wave. (b) The relative permittivity of LiF and NaCl.
Source: Data are taken by Palik [16].

length scales using self-organization of eutectic mixtures [32,33]. With this approach one can easily adjust the length-scale of the fabricated structures during the fabrication process, obtaining structures with different lattice-sizes and rod-diameters. The particular systems that we analyze here have been already fabricated, in different length scales, and their electromagnetic response has been experimentally studied using reflection and/or transmission measurements [31,34]. The geometrical characteristics of the fabricated systems are listed in Table 1.

The electromagnetic response of the fabricated structures has been studied also numerically and has been analyzed using effective medium formulas. Comparison with the experimental data showed that the response of the smaller of the systems can be reproduced and explained using the Maxwell-Garnett effective medium approach [35], summarized by Eq. (2) below, which is valid in the quasistatic regime, where the wavelength in both the rods and host is larger than the rod size and the lattice constant:

$$\varepsilon_{eff}^{\perp} = \varepsilon_{host}\frac{(1+\varphi)\varepsilon_{rods}+(1-\varphi)\varepsilon_{host}}{(1-\varphi)\varepsilon_{rods}+(1+\varphi)\varepsilon_{host}},$$
$$\varepsilon_{eff}^{\parallel} = \varphi\,\varepsilon_{rods}+(1-\varphi)\varepsilon_{host}. \quad (2)$$

In Eq. (2) φ is the rod filling ratio and the superscripts parallel and perpendicular refer to the electric field polarization relative to the rods axes – see Fig. 1(a). Regarding the larger-scale systems, they can also be described as effective media [36], but there more elaborated approaches should be employed, such as Pendry's averaging field approach [13,37], extended Maxwell-Garnett approach [38,39] and others [40]. This is due to the high-index response of the rods below the frequency ω_T (see Eq. (1)), which results to very short wavelengths inside the rods and thus to sub-wavelength Mie-resonances for even relatively small rod-diameters (note that the Mie-resonances of the rods appear when the wavelength inside the rods is comparable to the rod diameter) [14,41]. The requirement of effective medium approaches going beyond the quasi-static Maxwel-Garnett approach is quite common in the effective medium description of media composed of high index dielectrics.

In the discussion below we focus in most of the cases on the smallest among the fabricated structures mentioned in Table 1, and when effective medium description is required we employ the Maxwel-Garnett approach. For achieving detailed numerical data we employed the Microwave Studio commercial software, where the component material permittivity has been entered via the Lorenz model (Eq. (1)) with characteristic parameters as mentioned in Table 2. We have to mention here that the

Table 1
Geometrical characteristics of the fabricated alkali-halide systems that have been studied in this work. The rod diameters and lattice constants are measured average values. The structures exhibit deviations from the perfect regularity. For details see Ref. [31].

System	LiF volume fraction	Rod diameter (Lattice constant) [μm]
LiF rods in NaCl	25%	2.0 (3.6) to 10.7 (20.3)
LiF rods in KCl	6.9%	0.8 (2.8) to 6.4 (23.3)

Table 2
The characteristic frequencies appearing in the Lorenz (Eq. (1)) description of the component materials of the structures discussed here (ε_0 is the permittivity of the vacuum).

Material	Resonance frequency $f_T = \omega_T/2\pi$ [THz]	Longitudinal phonon frequency $f_L = \omega_L/2\pi$ [THz]	Damping frequency $\gamma' = \gamma/2\pi$ [THz]	Asymptotic relative permittivity $\varepsilon_\infty/\varepsilon_0$
LiF	9.22	19.1	0.527	2.027
NaCl	4.92	7.8	0.207	2.222
KCl	4.21	6.2	0.156	2.045

parameters of Table 2 for the LiF, while approaching very well the material response close to resonance frequency ω_T show slight deviation from the experimental permittivity values [16] around the frequency ω_L. This may result in small deviations in frequency of the phenomena discussed here if compared with future experimental data.

3. Hyperbolic dispersion relation in THz polaritonic metamaterials

Structures with hyperbolic dispersion relation, known as hyperbolic metamaterials [42,43], have been proved recently as a very important category of metamaterials, since they show the ability for subwavelength resolution imaging (known as hyperlensing [44]) without the need for resonant response (which implies high losses) or magnetic response (which is not easy to be achieved, especially in high frequencies), while they offer an easy practical realization due to the simple geometries involved. Such metamaterials are uniaxial anisotropic structures with one principal component of the effective permittivity (or permeability) negative and the others positive, resulting to equifrequency surfaces (i.e. surfaces of constant frequency in **k**-space) of the shape of hyperbola (unlike the ellipsoid-like surfaces of metamaterials with all the permittivity (or permeability) components being of the same sign) [45]. The easier practical realization of such metamaterials is encountered in systems of negative permittivity (e.g. metallic) rods periodically placed in a dielectric host, or in lamellar (multilayer) systems alternating negative and positive permittivity layers (i.e. metal-dielectric layers) [43]. Here we demonstrate hyperbolic metamaterial response in polaritonic systems.

The ability of hyperbolic metamaterials (HMM) for subwavelength resolution imaging is based on the fact the HMM do not have an upper limit in the magnitude of propagating wave vectors that they can support (due to the unbounded form of the hyperbola, in contrast to ellipsoid or sphere), so they can transmit arbitrarily large (in principle) wave vectors [44,46]. In a regular medium, wavevector components larger than $\omega n/c$ (n is the refractive index of a medium and c the vacuum wave velocity) along one direction correspond to evanescent waves along the perpendicular direction and are lost if propagation occurs in regular media. These components though, which carry the finest details of the source object emitting them (forming the basis of Pendry's superlens [11]), can be coupled to propagating waves in a HMM and transmitted without attenuation (beyond the attenuation associated with the losses of the materials) [46,47]. Besides the subwavelength resolution imaging, the hyperbolic dispersion is associated also with broadband high density of EM modes, which can greatly affect the performance of EM sources placed in HMM [48–50]. Other interesting possibilities that can also be realized in HMMs are advanced absorption and thermal emission control [51,52], cloaking possibilities [53], possibilities to mimic phenomena related to gravitation theory [54] etc.

HMM have been realized so far in the IR and optical regime using periodic systems of metallic rods in a host [55–57] or metallic layered systems [58,59], and subwavelength resolution imaging has been demonstrated, even associated with image magnification when the layers are properly curved [44] (for a review see Ref. [43]). Here we show that the same effects can be observed in the THz regime in systems of polaritonic rods in a host, exploiting the negative permittivity response of the rods [31,36]. Such a system is the LiF rods in NaCl host system shown in Fig. 1(a), in the frequency region between 9.5 and ~13 THz. Applying the Maxwell-Garnet effective medium formula (Eq. (2)) for such a system, which, as we mentioned earlier, is valid for rod diameters smaller than 2 microns, one achieves the effective permittivity response shown in Fig. 2. The permittivity of Fig. 2 for the frequency region 9.5–13 THz shows negative values for electric field (**E**) parallel to the rods and positive for **E** perpendicular to the rods (see Fig. 1(a) for the description of polarization), suggesting hyperbolic metamaterial response. Selecting an interface

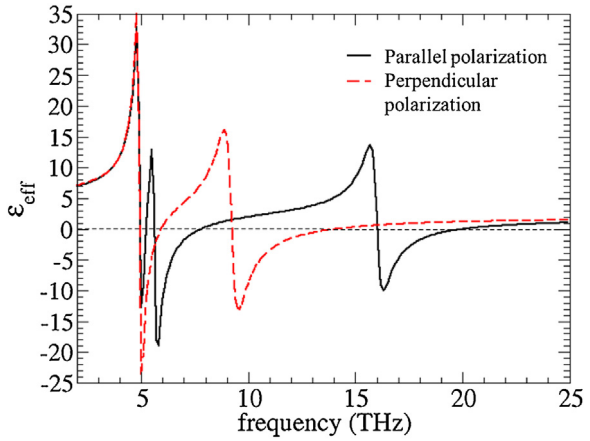

Fig. 2. Effective relative permittivity for a system of parallel infinitely long LiF rods embedded in NaCl, for LiF volume fraction 25%, and for the two different possible polarizations of an incident EM field relative to the rod axes (see Fig. 1(a)). The effective permittivity was calculated using the Maxwel-Garnett effective medium formulas (Eq. (2)), where for the permittivity of the component materials the Lorenz approximation of the data presented in Fig. 1(b) was used, with parameters those listed in Table 2.

perpendicular to the rods (see Fig. 3(b)) and calculating the dispersion curves k_{parallel} vs $k_{\text{perpendicuar}}$, where the parallel and perpendicular here refer to the interface, one achieves the curves shown in Fig. 3(a), demonstrating the hyperbolic dispersion relation response.

This hyperbolic dispersion relation and the resulting possibility for subwavelength resolution imaging in our LiF in NaCl system was demonstrated also in detailed numerical simulations. An example is shown in Fig. 3(b), where a localized source emitting a TM wave is placed close to the interface between air and the LiF–NaCl system, and imaging with resolution ∼λ/4 is demonstrated for frequency 10.86 THz. Note that the system length here is chosen as to match the effective wavelength in the system, exploiting thus the Fabry-Perot resonances of the system, which allow maximum transmission.

One has to point here that the employment of polaritonic materials as a means to achieve hyperbolic dispersion relation response is associated with certain advantages, compared to corresponding metallic systems: (a) In polaritonic systems one avoids the problem of spatial dispersion which is common in metallic structures operating in microwaves and THz and complicates the structure response [60,61]. (b) The loss factor, Im(ε)/Re(ε), of polaritonic materials in the frequency region of hyperbolic dispersion is smaller (it is of the order of 10) than that of metals in the optical region (where the permittivity values are similar), allowing larger propagation distances in THz polaritonic metamaterials than in similar nanoscale metallic systems. This, combined with the much easier experimental realization of the THz polaritonic structures, shows that such structures offer an ideal system for demonstration and analysis of the effects and possibilities associated with hyperbolic dispersion relation.

4. THz superlensing based on backward radiation in negative permittivity waveguides

Waveguides made of polaritonic materials possess some unique properties unattainable by other materials in the THz frequency range, due to the small negative permittivity values that polaritonic materials possess as the frequency approaches ω_L. In waveguides with small

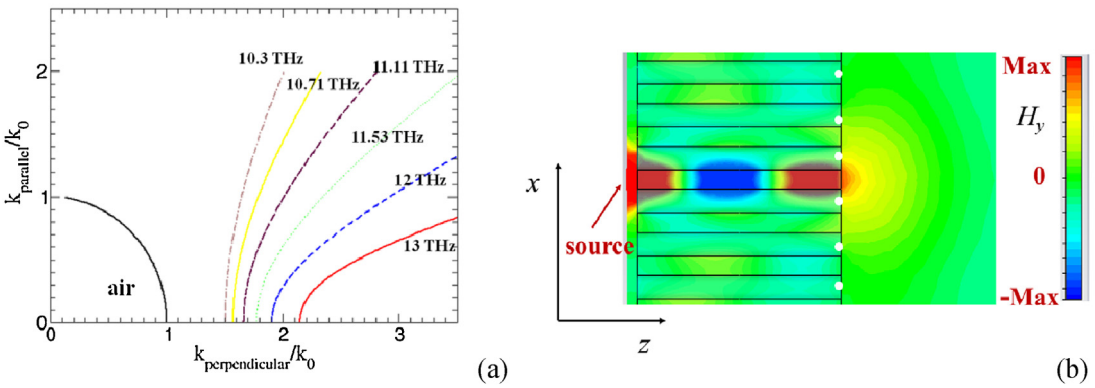

Fig. 3. (a) Dispersion curves for the extraordinary wave propagating along the rods in the LiF in NaCl metamaterial studied (see Fig. 1(a)); (b) demonstration of superlensing in that metamaterial by showing the magnetic field component H_y propagating along the structure. k_{parallel} is the **k**-component parallel to the interface between air and the metamaterial, i.e. along x-direction of panel (b), and $k_{\text{perpendicuar}}$ is along z-direction. The incident wave in panel (b) is a TM wave (magnetic field along y-direction and electric field in the x–z plane) of frequency 10.86 THz. The diameter of the LiF rods in the system is 2 μm and the lattice constant of the hexagonal lattice 10.7 μm. To distinguish between rods and host stripes in the two-dimensional cross-section of the system presented in panel (b) we have marked the rod position by white dots.

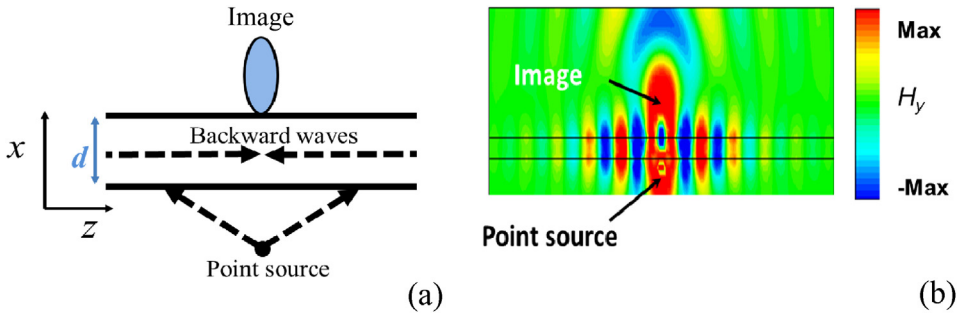

Fig. 4. (a) Scheme of the focusing mechanism based on backward propagated and radiating guided modes; (b) magnetic field component H_y field distribution in a LiF slab of thickness $d = 2$ μm embedded in NaCl at frequency 13.5 THz. The source is a TM point source (magnetic field along y) located 1 μm away from the LiF–NaCl interface.

negative permittivity values there is the possibility of backward guided modes (i.e. modes of opposite phase and group velocity) which show quite strong leakage outside the guide, leading to backward radiation from the side-walls of the guide [62].

To understand this better let's consider a planar slab waveguide of relative permittivity ε_1 and thickness d (along x-direction – infinite along y and z directions – see Fig. 4(a)) embedded in a material of relative permittivity ε_2. For TM electromagnetic modes (i.e. magnetic field in the plane of the slab boundaries) the dispersion relation of the even guided modes (i.e. modes propagating along the guide and evanescent outside the guide, along x-direction) [62] is

$$k_{2x}d = k_{1x}d\frac{\varepsilon_2}{\varepsilon_1}\tan(k_{1x}d), \quad \text{with}$$
$$k_{1x} = \sqrt{k_0^2\varepsilon_1 - q^2}, \quad k_{2x} = \sqrt{q^2 - k_0^2\varepsilon_2}. \qquad (3)$$

In Eq. (3), $k_0 = \omega/c$, q is the wave-vector component along the waveguide, which is continuous across the guide boundaries, and the subscripts in the **k**-components denote the medium (1 for the waveguide, 2 for the surrounding medium) and the direction. Using the above equations to solve the dispersion relation q vs k_0, one can find for $\varepsilon_1 < 0$ the existence of backward "guided" waves, which have also a large attenuation component (Im(q)) along the direction of the guide, indicating leakage outside the guide across the guide boundaries. For large negative values of ε_1 these waves do not dominate the flux propagating along the guide, but under certain conditions, e.g. for small negative values of ε_1 (as compared in magnitude to ε_2) these backward waves dominate the guided flux and, due to the conservation of q, lead to negatively refracted leaking waves, i.e. backward radiation outside the guide along the x-direction. Thus if one places a point source outside a waveguide having small negative permittivity values, as to excite the backward guided modes, the negatively refracted leaking waves converge at the other side of the guide (see Fig. 4) resulting to an image of the point source; this makes the guide operating as a flat lens, providing also subwavelength resolution due to the restoration of the evanescent waves emitted by the source.

Exploiting further the backward radiating modes mentioned above, one can achieve subwavelength imaging (or subwavelenth tunneling of electromagnetic waves) in a system of parallel cylindrical waveguides, such as the LiF rods (acting as waveguides) in NaCl host system, which was discussed in the previous section, in the frequency regime around 16 THz where LiF has small negative epsilon values and NaCl behaves as a dielctric [16]. Such a subwavelength imaging is numerically demonstrated in Fig. 5.

To distinguish between rods and host stripes in the two-dimensional cross-section of the system presented in panel (b) we have marked the rod position by white dots.

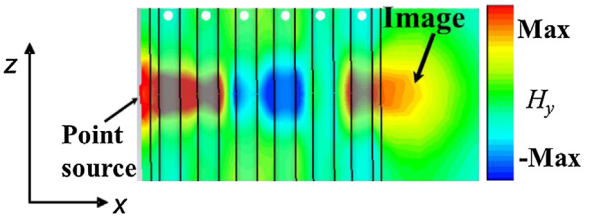

Fig. 5. Subwavelength propagation and imaging due to backward radiation in the system of LiF rods in NaCl that was discussed in Section III and Fig. 3, in the frequency region of small negative LiF permittivity (here 16.24 THz). The propagation along z-direction in the LiF rods is backward leading to convergence of the leaked radiation in the NaCl host due to negative refraction. The point source emits a TM wave (magnetic field along y-direction), and figure shows the magnetic field component H_y. The white dots in the figure are used to mark the position of the rods, as described also in Fig. 3.

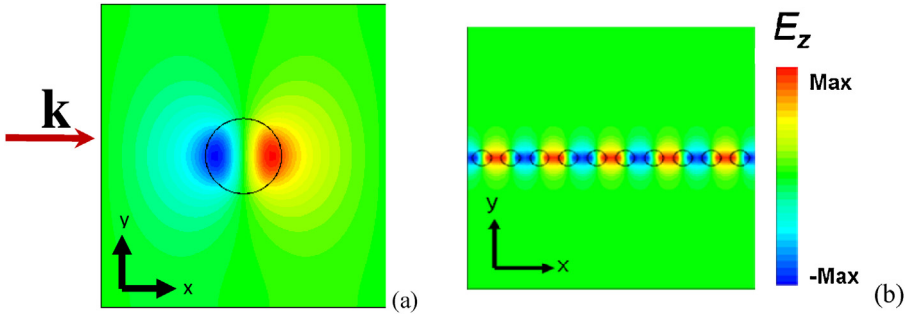

Fig. 6. (a) The scattered electric field by a dielectric cylinder (of relative permittivity 40 and radius 4 μm) embedded in an ENZ medium at the region of a cylinder resonance (4.54 THz). The electric field in the incoming wave is parallel to the cylinder. (b) Very confined almost perfect propagation along an array of dielectric cylinders (as the one shown in panel (a)) embedded in an ENZ medium due to the p-like symmetry of each individual scattered field. The guiding occurs at frequency 4.55 THz, i.e. almost identical to the frequency of a Mie-resonance.

5. Epsilon near zero based total transmission and subwavelength guiding in polaritonic systems

As was mentioned in the introduction, one can achieve a variety of interesting phenomena in media with epsilon near zero; this is mainly due to propagation with practically no phase advance that can take place in such media [26,63,64]. Even more interesting and rich phenomena can be observed if one combines properly *structured* ENZ media with normal dielectrics [65,66]. For example, inserting regular dielectric scatterers in an ENZ medium one can observe similar phenomena to the ones achieved in media composed of *high-index* dielectric scatterers in a regular dielectric host, such as negative permeability and/or permittivity. This is due to the large wavelength in the ENZ host (allowing the scatterer's Mie-resonances to occur in subwavelength regions) and the too high contrast in the dielectric parameters between scatterers and the ENZ host. Other interesting phenomena occurring in media with scatterers in an ENZ host are total transmission or total reflection or EM cloaking for TM incident wave polarization if the scatterers are made of a PEC material [67], and, as was shown recently, total transmission and extreme subwavelength guiding of TE polarized waves in media with cylindrical dielectric scatteres in an ENZ host [30,34].

The presence of epsilon near zero frequency regions in polaritonic materials, combined with the easiness in the fabrication of composite media made of polaritonic materials, allows the easy observation and exploitation in THz of all the interesting phenomena that can observed in composite media of scatteres in ENZ host. We showed recently that such interesting phenomena are extreme subwavelength guiding associated with total EM wave transmission [30,34].

Analyzing the propagation of a plane electromagnetic wave coming from vacuum and impinging on an ENZ medium with embedded dielectric cylinders [30], for **E** parallel to the cylinders one can observe extremely subwavelength and strongly confined Mie-resonances in the cylinders, where the electric field distribution shows the symmetry of p-like atomic orbitals oriented along the direction of the incident wave (see Fig. 6(a)). It can be shown both analytically and numerically [30] that the presence of such resonances: (a) maximizes the coupling of the resonators along propagation direction if cylindrical resonators are placed next to each other, and (b) can result in almost total transmission of the incident wave by the system.

These effects can be exploited in an ordered linear arrangement of dielectric cylinders placed in an ENZ host, as shown in Fig. 6(b). Such an arrangement acts as a narrow subwavelength channel where the wave propagates by being transferred from scatterer to scatterer,

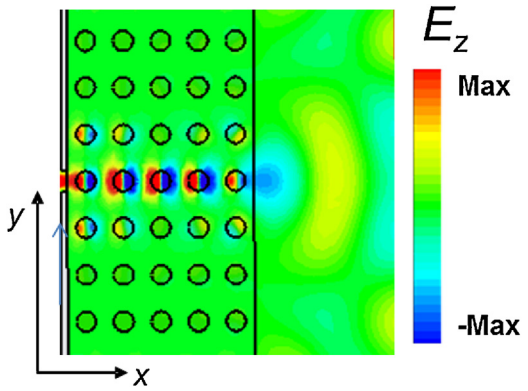

Fig. 7. Subwavelength guiding exploiting the Mie-resonances of LiF rods in NaCl, at frequency 7.85 THz where NaCl has permittivity near zero and LiF relative permittivity 24.8. The guiding is demonstrated by showing the electric field component E_z of an incident wave coming from a slit on PEC screen. The rod diameter here is 6.4 μm and the lattice constants are 12 μm along x-direction and 15 μm along y.

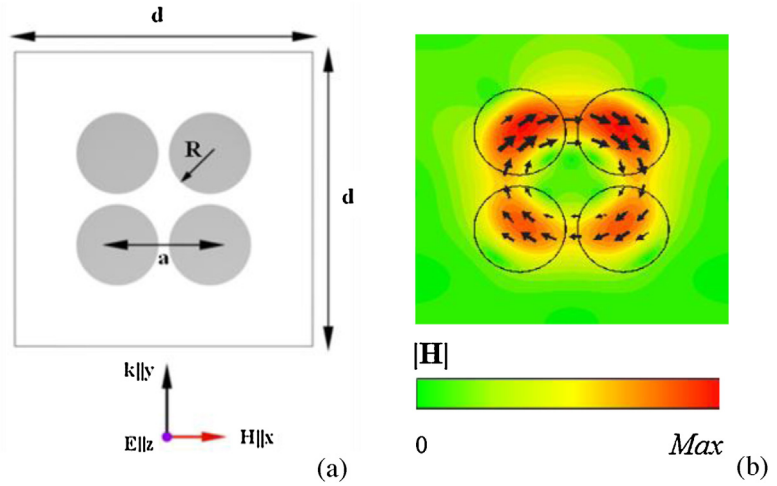

Fig. 8. (a) A dielectric metamolecule supporting toroidal dipolar response for the incident electromagnetic field configuration shown in the figure. The metamolecule is a cluster of 4 infinitely long cylinders of radius $R = 8$ μm and center-to-center separation $a = 18$ μm. The metamaterial is formed by placing the metamolecules periodically along the x-axis with period $d = 58$ μm. (b) Calculated distribution of the absolute value of the magnetic field induced in the metamolecule of panel (a), made by $LiTaO_3$ rods at frequency 1.89 THz. The arrows show the magnetic flux.

forming an extremely subwavelength and efficient (i.e. of high transmission) waveguide.

Subwavelength guiding due to Mie-resonances in ENZ host can be sustained even in two-dimensional periodic systems, such as the LiF rods in NaCl host at the ENZ response region of the host, since the coupling of the neighboring cylinders along propagation direction dominates (due to the directional form of the resonant fields). Fig. 7 demonstrates this response for a 2D rectangular periodic system of LiF rods in NaCl, at frequency 7.85 THz where NaCl behaves as an ENZ material. Subwavelength guiding with enhanced transmission due to ENZ host has been also demonstrated in periodic systems of LiF rods in KCl as the ones described in Table 1; there, the transmission, which was studied also experimentally, showed a peak at the ENZ region of KCl (despite the large thickness of the system and the non-perfect regularity), confirming the possibility for high transmission due to ENZ host response [34].

6. Toroidal response in eutectic metamaterials

Besides metamaterials made of periodically placed individual rods, metamaterials consisting of clusters of rods, or more generally clusters of scatterers, as basic building blocks can also provide very interesting effects. Such effects that have been already demonstrated are Fano resonances in plasmonic clusters and in clusters made of high index dielectric particles [68,69], ultrastrong electromagnetic field localization inside clusters of particles, leading to enhancement of non-linearities [70], etc.

As it has been shown recently, a particularly interesting effect that becomes possible in properly shaped clusters of high index dielectric cylinders (see Fig. 8) is toroidal dipolar response [71–73]. Toroidal dipolar response is created by currents circulating on a surface of a torus perpendicular to its axis, resulting in a magnetic flux having the shape of a torus [74]. Such a response, although it results from an elementary current excitation, is usually omitted from the standard multipole analysis; it is associated though with a multitude of unusual and interesting phenomena, such as non-reciprocal refraction of light [75], generation of vector potentials without presence of electric fields [76], etc.

In the context of metamaterials toroidal response has been demonstrated so far by using clusters of metallic elements, such like split-ring resonator clusters [74,77–79]. Only recently the realization of such response in high index dielectrics was demonstrated [71], specifically in systems composed of torus-like-shaped clusters of high index dielectric rods, as shown in Fig. 8(a). This demonstration, combined with a relevant analysis on the toroidal response of high index dielectrics, suggests that the most natural platform for practical realization of toroidal response in the THz region is a system of polaritonic rods, such as $LiTaO_3$ rods, which exhibit large permittivity values even well below the phonon resonance frequency ω_T – see Eq. (1). Note that for $LiTaO_3$ $\omega_T/2\pi = 26.7$ THz, $\omega_L/2\pi = 46.9$, $\gamma/2\pi = 0.94$ THz and $\varepsilon_\infty/\varepsilon_0 = 13.4$ [20].

At frequencies of few THz, which lie well below the phonon resonance frequency ω_T, the relative permittivity of $LiTaO_3$ is still high, reaching $\varepsilon = 41.4$ and allowing thus the demonstration of toroidal response in systems like the one of Fig. 8(a), where the meta-molecule is composed of 4 closely placed and aligned cylinders. In Fig. 8(b) we demonstrate the toroidal response in such a system (made of by $LiTaO_3$ rods) by plotting the magnetic field and the resulting magnetic flux in the meta-molecule shown in Fig. 8(a). The torus-like shape of the magnetic flux is a demonstration of the toroidal response which was further confirmed by comparing simulations data with results of analysis based on multiplole expansion of scattered fields [71].

7. Conclusions

Materials exhibiting a phonon-polariton resonance (polaritonic materials) offer unique possibilities in metamaterial-based phenomena and applications, as a result of the rich permittivity response that they exhibit, ranging from large positive to large negative and near zero values, combined with their THz operation regime, where most of the natural materials do not show strong response.

Here we discussed metamaterials composed of cylindrical rods in a host where both rods and host are made of a polaritonic material. We demonstrated numerically a variety of phenomena and possibilities in such metamaterials, including hyperbolic dispersion relation response, suitable for superlensing, backward radiation, also suitable for superlensing, total transmission and subwavelength guiding exploiting Mie-resonances of the rods at the ENZ response of the host, as well as toroidal response. Many more possibilities can be realized and demonstrated at the same system, including negative permeability and/or permittivity, and even negative refractive index, controlled absorption, high-field confinement appropriate for biomolecular sensing, etc.

The study presented here was inspired and prompted mainly by the easy practical realization of the above mentioned metamaterials, by employing self-organization of alkali-halide eutectic systems. This approach is fast, cost-effective, and allows adjustment of the length scale of the structure at the time of fabrication, offering extensive possibilities in shapes, sizes and materials involved.

The observation of such a rich variety of phenomena as the ones mentioned above in only one particular geometrical configuration is a clear indication for the huge possibilities offered by polaritonic materials in connection to metamaterials. This is especially true in view of polaritonic material's operation in the THz region, where, in spite of the needs, there is a significant gap in observed phenomena, appropriate materials, and devices. THz polaritonic metamaterials seem capable to fill-in the gap, to stimulate new devices, and to open the path for unique potential applications.

Acknowledgements

Authors acknowledge financial support by EU project ENSEMBLE (Grant Agreement No. 213669) and by Greek GSRT through the project ERC-02 EXEL. Work at Ames Laboratory was partially supported by the U.S. Department of Energy (Basic Energy Sciences, Division of Materials Sciences and Engineering), Contract No. DE-AC02-07CH11358, and by the US Office of Naval Research (Award No. N00014-10-1-0925).

References

[1] Y.-S. Lee, Principles of Terahertz Science and Technology, Springer US, Boston, MA, 2008.
[2] X.-C. Zhang, J. Xu, Introduction to THz Wave Photonics, Springer, New York, 2009.
[3] J.B. Pendry, A.J. Holden, D.J. Robbins, W.J. Stewart, Magnetism from conductors and enhanced nonlinear phenomena, IEEE Trans. Microw. Theory Techn. 47 (1999) 2075–2084.
[4] V.G. Veselago, The electrodynamics of substances with simultaneously negative values of ε and μ, Sov. Phys. Uspekhi 10 (1968) 509.
[5] R.A. Shelby, D.R. Smith, S. Schultz, Experimental verification of a negative index of refraction, Science 292 (2001) 77–79.
[6] Z.F. Li, M. Mutlu, E. Ozbay, Chiral metamaterials: from optical activity and negative refractive index to asymmetric transmission, J. Opt. 15 (2013) 023001.
[7] B.N. Wang, J.F. Zhou, T. Koschny, M. Kafesaki, C.M. Soukoulis, Chiral metamaterials: simulations and experiments, J. Opt. A: Pure Appl. Opt. 11 (2009).
[8] N.I. Zheludev, The road ahead for metamaterials, Science 328 (2010) 582–583.
[9] C.M. Watts, X.L. Liu, W.J. Padilla, Metamaterial electromagnetic wave absorbers, Adv. Mater. 24 (2012) OP98–OP120.
[10] G.C.R. Devarapu, S. Foteinopoulou, Mid-IR near-perfect absorption with a SiC photonic crystal with angle-controlled polarization selectivity, Opt. Express 20 (2012) 13040–13054.
[11] J.B. Pendry, Negative refraction makes a perfect lens, Phys. Rev. Lett. 85 (2000) 3966–3969.
[12] J.K. Gansel, M. Thiel, M.S. Rill, M. Decker, K. Bade, V. Saile, G. von Freymann, S. Linden, M. Wegener, Gold helix photonic metamaterial as broadband circular polarizer, Science 325 (2009) 1513–1515.
[13] S. O'Brien, J.B. Pendry, Photonic band-gap effects and magnetic activity in dielectric composites, J. Phys.: Condens. Matter 14 (2002) 4035.
[14] Q. Zhao, J. Zhou, F.L. Zhang, D. Lippens, Mie resonance-based dielectric metamaterials, Mater. Today 12 (2009) 60–69.

[15] N.W. Ashcroft, N.D. Mermin, Solid State Physic Holt, Rinehart and Winston, New York, USA, 1976.
[16] E.D. Palik, Handbook of Optical Constants of Solids, Elsevier Inc., 1997.
[17] K.C. Huang, P. Bienstman, J.D. Joannopoulos, K.A. Nelson, S.H. Fan, Field expulsion and reconfiguration in polaritonic photonic crystals (vol. 90, art. no. 196402, 2003), Phys. Rev. Lett. 92 (2004).
[18] D.Z.A. Chen, R. Hamam, M. Soljacic, J.D. Joannopoulos, G. Chen, Extraordinary optical transmission through subwavelength holes in a polaritonic silicon dioxide film, Appl. Phys. Lett. 90 (2007).
[19] V. Myroshnychenko, A. Stefanski, A. Manjavacas, M. Kafesaki, R.I. Merino, V.M. Orera, D.A. Pawlak, F.J. García de Abajo, Interacting plasmon and phonon polaritons in aligned nano- and microwires, Opt. Express 20 (2012) 10879–10887.
[20] K.C. Huang, M.L. Povinelli, J.D. Joannopoulos, Negative effective permeability in polaritonic photonic crystals, Appl. Phys. Lett. 85 (2004).
[21] J.A. Schuller, R. Zia, T. Taubner, M.L. Brongersma, Dielectric metamaterials based on electric and magnetic resonances of silicon carbide particles, Phys. Rev. Lett. 99 (2007) 107401.
[22] L. Peng, L.X. Ran, H.S. Chen, H.F. Zhang, J.A. Kong, T.M. Grzegorczyk, Experimental observation of left-handed behavior in an array of standard dielectric resonators, Phys. Rev. Lett. 98 (2007).
[23] M.S. Wheeler, J.S. Aitchison, M. Mojahedi, Three-dimensional array of dielectric spheres with an isotropic negative permeability at infrared frequencies, Phys. Rev. B 72 (2005) 193103.
[24] I.K.L. Jylhä, S. Maslovski, S. Tretyakov, Modeling of isotropic backward-wave materials composed of resonant spheres, J. Appl. Phys. 99 (2006).
[25] M. Silveirinha, N. Engheta, Tunneling of electromagnetic energy through subwavelength channels and bends using epsilon near-zero materials, Phys. Rev. Lett. 97 (2006) 157403.
[26] M.G. Silveirinha, N. Engheta, Theory of supercoupling, squeezing wave energy, and field confinement in narrow channels and tight bends using epsilon near-zero metamaterials, Phys. Rev. B 76 (2007).
[27] A. Alù, M.G. Silveirinha, A. Salandrino, N. Engheta, Epsilon-near-zero metamaterials and electromagnetic sources: tailoring the radiation phase pattern, Phys. Rev. B 75 (2007) 155410.
[28] O. Sydoruk, E. Shamonina, V. Kalinin, L. Solymar, Terahertz instability of surface optical-phonon polaritons that interact with surface plasmon polaritons in the presence of electron drift, Phys. Plasmas 17 (2010).
[29] O. Sydoruk, V. Kalinin, L. Solymar, Terahertz instability of optical phonons interacting with plasmons in two-dimensional electron channels, Appl. Phys. Lett. 97 (2010).
[30] A.A. Basharin, C. Mavidis, M. Kafesaki, E.N. Economou, C.M. Soukoulis, Epsilon near zero based phenomena in metamaterials, Phys. Rev. B 87 (2013) 155130.
[31] A. Reyes-Coronado, M.F. Acosta, R.I. Merino, V.M. Orera, G. Kenanakis, N. Katsarakis, M. Kafesaki, C. Mavidis, J.G. de Abajo, E.N. Economou, C.M. Soukoulis, Self-organization approach for THz polaritonic metamaterials, Opt. Express 20 (2012) 14663–14682.
[32] D.A. Pawlak, Metamaterials and photonic crystals – potential applications for self-organized eutectic micro- and nanostructures, Sci. Plena 4 (2008) 014801.
[33] R.I. Merino, M.F. Acosta, V.M. Orera, New polaritonic materials in the THz range made of directionally solidified halide eutectics, J. Eur. Ceram. Soc. (2013).
[34] M. Massaouti, A.A. Basharin, M. Kafesaki, M.F. Acosta, R.I. Merino, V.M. Orera, E.N. Economou, C.M. Soukoulis, S. Tzortzakis, Eutectic epsilon-near-zero metamaterial terahertz waveguides, Opt. Lett. 38 (2013) 1140–1142.
[35] A. Sihvola, Electromagnetic Mixing Formulae and Applications.
[36] S. Foteinopoulou, M. Kafesaki, E.N. Economou, C.M. Soukoulis, Two-dimensional polaritonic photonic crystals as terahertz uniaxial metamaterials, Phys. Rev. B 84 (2011) 035128.
[37] D.R. Smith, J.B. Pendry, Homogenization of metamaterials by field averaging (invited paper), J. Opt. Soc. Am. B: Opt. Phys. 23 (2006) 391–403.
[38] R. Ruppin, Evaluation of extended Maxwel-Garnett theories, Opt. Commun. 182 (2000) 273–279.
[39] V. Yannopapas, Negative refraction in random photonic alloys of polaritonic and plasmonic microspheres, Phys. Rev. B 75 (2007).
[40] V. Yannopapas, Effective-medium description of disordered photonic alloys, J. Opt. Soc. Am. B: Opt. Phys. 23 (2006) 1414–1419.
[41] J.A. Stratton, Electromagnetic Theory, McGraw-Hill, New York, 1941.
[42] M. Noginov, M. Lapine, V. Podolskiy, Y. Kivshar, Focus issue: hyperbolic metamaterials, Opt. Express 21 (2013) 14895–14897.
[43] A. Poddubny, I. Iorsh, P. Belov, Y. Kivshar, Hyperbolic metamaterials, Nat. Photonics 7 (2013) 10.
[44] Z.W. Liu, H. Lee, Y. Xiong, C. Sun, X. Zhang, Far-field optical hyperlens magnifying sub-diffraction-limited objects, Science 315 (2007) 1686.
[45] A. Fang, T. Koschny, C.M. Soukoulis, Optical anisotropic metamaterials: negative refraction and focusing, Phys. Rev. B 79 (2009).
[46] Z. Jacob, L.V. Alekseyev, E. Narimanov, Optical hyperlens: far-field imaging beyond the diffraction limit, Opt. Express 14 (2006) 8247–8256.
[47] X. Zhang, Z.W. Liu, Superlenses to overcome the diffraction limit, Nat. Mater. 7 (2008) 435–441.
[48] Z. Jacob, J.Y. Kim, G.V. Naik, A. Boltasseva, E.E. Narimanov, V.M. Shalaev, Engineering photonic density of states using metamaterials, Appl. Phys. B: Lasers Opt. 100 (2010) 215–218.
[49] Z. Jacob, I.I. Smolyaninov, E.E. Narimanov, Broadband Purcell effect: radiative decay engineering with metamaterials, Appl. Phys. Lett. 100 (2012).
[50] J. Kim, V.P. Drachev, Z. Jacob, G.V. Naik, A. Boltasseva, E.E. Narimanov, V.M. Shalaev, Improving the radiative decay rate for dye molecules with hyperbolic metamaterials, Opt. Express 20 (2012) 8100–8116.
[51] T.U. Tumkur, L. Gu, J.K. Kitur, E.E. Narimanov, M.A. Noginov, Control of absorption with hyperbolic metamaterials, Appl. Phys. Lett. 100 (2012).
[52] Y. Guo, Z.B. Jacob, Thermal hyperbolic metamaterials, Opt. Express 21 (2013) 15014–15019.
[53] V.P. Drachev, V.A. Podolskiy, A.V. Kildishev, Hyperbolic metamaterials: new physics behind a classical problem, Opt. Express 21 (2013) 15048–15064.
[54] I.I. Smolyaninov, Y.J. Hung, Minkowski domain walls in hyperbolic metamaterials, Phys. Lett. A 377 (2013) 353–356.
[55] J.F. Einsle, G. Scheunert, A. Murphy, J. McPhillips, A.V. Zayats, R. Pollard, R.M. Bowman, Directed self-assembly of nanorod networks: bringing the top down to the bottom up, Nanotechnology 23 (2012).
[56] A.V. Kabashin, P. Evans, S. Pastkovsky, W. Hendren, G.A. Wurtz, R. Atkinson, R. Pollard, V.A. Podolskiy, A.V. Zayats, Plasmonic nanorod metamaterials for biosensing, Nat. Mater. 8 (2009) 867–871.

[57] M.A. Noginov, Y.A. Barnakov, G. Zhu, T. Tumkur, H. Li, E.E. Narimanov, Bulk photonic metamaterial with hyperbolic dispersion, Appl. Phys. Lett. 94 (2009).
[58] T. Tumkur, G. Zhu, P. Black, Y.A. Barnakov, C.E. Bonner, M.A. Noginov, Control of spontaneous emission in a volume of functionalized hyperbolic metamaterial, Appl. Phys. Lett. 99 (2011).
[59] H.N.S. Krishnamoorthy, Z. Jacob, E. Narimanov, I. Kretzschmar, V.M. Menon, Topological transitions in metamaterials, Science 336 (2012) 205–209.
[60] A.V. Chebykin, A.A. Orlov, C.R. Simovski, Y.S. Kivshar, P.A. Belov, Nonlocal effective parameters of multilayered metal-dielectric metamaterials, Phys. Rev. B 86 (2012).
[61] P.A. Belov, R. Marques, S.I. Maslovski, I.S. Nefedov, M. Silveirinha, C.R. Simovski, S.A. Tretyakov, Strong spatial dispersion in wire media in the very large wavelength limit, Phys. Rev. B 67 (2003).
[62] A.A. Basharin, M. Kafesaki, E.N. Economou, C.M. Soukoulis, Backward wave radiation from negative permittivity waveguides and its use for THz subwavelength imaging, Opt. Express 20 (2012) 12752–12760.
[63] M. Silveirinha, N. Engheta, Tunneling of electromagnetic energy through subwavelength channels and bends using epsilon-near-zero materials, Phys. Rev. Lett. 97 (2006).
[64] A. Alu, M.G. Silveirinha, A. Salandrino, N. Engheta, Epsilon-near-zero metamaterials and electromagnetic sources: tailoring the radiation phase pattern, Phys. Rev. B 75 (2007).
[65] Y. Xu, H. Chen, Total reflection and transmission by epsilon-near-zero metamaterials with defects, Appl. Phys. Lett. 98 (2011) 113501–113503.
[66] V.C. Nguyen, L. Chen, K. Halterman, Total transmission and total reflection by zero index metamaterials with defects, Phys. Rev. Lett. 105 (2010) 233908.
[67] J.M. Hao, W. Yan, M. Qiu, Super-reflection and cloaking based on zero index metamaterial, Appl. Phys. Lett. 96 (2010).
[68] A.E. Miroshnichenko, Y.S. Kivshar, Fano resonances in all-dielectric oligomers, Nano Lett. 12 (2012) 6459–6463.
[69] B. Hopkins, A.N. Poddubny, A.E. Miroshnichenko, Y.S. Kivshar, Revisiting the physics of Fano resonances for nanoparticle oligomers, Phys. Rev. A 88 (2013) 10.
[70] H. Merbold, A. Bitzer, T. Feurer, Second harmonic generation based on strong field enhancement in nanostructured THz materials, Opt. Express 19 (2011) 7262–7273.
[71] A.A. Basharin, M. Kafesaki, E.N. Economou, C.M. Soukoulis, V.A. Fedotov, V. Savinov, N.I. Zheludev, Dielectric metamaterials with toroidal dipolar response, Phys. Rev. (2014).
[72] V.A. Fedotov, A.V. Rogacheva, V. Savinov, D.P. Tsai, N.I. Zheludev, Non-trivial non-radiating excitation as a mechanism of resonant transparency in toroidal metamaterials, Phys. Opt. (2012).
[73] V. Savinov, V.A. Fedotov, N.I. Zheludev, Toroidal dipolar excitation and macroscopic electromagnetic properties of metamaterials, Phys. Rev. B 89 (20) (2014) 205112.
[74] T. Kaelberer, V.A. Fedotov, N. Papasimakis, D.P. Tsai, N.I. Zheludev, Toroidal dipolar response in a metamaterial, Science 330 (2010) 1510–1512.
[75] K. Sawada, N. Nagaosa, Optical magnetoelectric effect in multiferroic materials: evidence for a Lorentz force acting on a ray of light, Phys. Rev. Lett. 95 (2005) 237402.
[76] G.N. Afanasiev, Y.P. Stepanovsky, The electromagnetic-field of elementary time-dependent toroidal sources, J. Phys. A: Math. Gen. 28 (1995) 4565–4580.
[77] Z.-G. Dong, P. Ni, J. Zhu, X. Yin, X. Zhang, Toroidal dipole response in a multifold double-ring metamaterial, Opt. Express 20 (2012) 13065–13070.
[78] Z.G. Dong, J. Zhu, J. Rho, J.Q. Li, C.G. Lu, X.B. Yin, X. Zhang, Optical toroidal dipolar response by an asymmetric double-bar metamaterial, Appl. Phys. Lett. 101 (2012).
[79] Y. Fan, Z. Wei, H. Li, H. Chen, C.M. Soukoulis, Low-loss and high-Q planar metamaterial with toroidal moment, Phys. Rev. B 87 (2013) 115417.